ACS OMEGA

http://pubs.acs.org/journal/acsodf

Article

Investigation of a Dual siRNA/Chemotherapy Delivery System for Breast Cancer Therapy

Yongmei Zhao,[#] Tianqing Liu,[#] Aditya Ardana, Nicholas L. Fletcher, Zachary H. Houston, Idriss Blakey, and Kristofer J. Thurecht*

Cite This: *ACS Omega* 2022, 7, 17119−17127

Read Online

ACCESS | Metrics & More | Article Recommendations | Supporting Information

ABSTRACT: Multidrug resistance (MDR) is a problem that is often associated with a poor clinical outcome in chemotherapeutic cancer treatment. MDR may potentially be overcome by utilizing synergistic approaches, such as combining siRNA gene therapy and chemotherapy to target different mechanisms of apoptosis. In this study, a strategy is presented for developing multicomponent nanomedicines using orthogonal and compatible chemistries that lead to effective nanotherapeutics. Hyperbranched polymers were used as drug carriers that contained doxorubicin (DOX), attached via a pH-sensitive hydrazone linkage, and ataxia-telangiectasia mutated (ATM) siRNA, attached via a redox-sensitive disulfide group. This nanomedicine also contained cyanine 5 (Cy5) as a diagnostic tracer as well as in-house developed bispecific antibodies that allowed targeting of the epidermal growth factor receptor (EGFR) present on tumor tissue. Highly efficient coupling of siRNA was achieved with 80% of thiol end-groups on the hyperbranched polymer coupling with siRNA. This attachment was reversible, with the majority of siRNA released *in vitro* under reducing conditions as desired. In cellular studies, the nanomedicine exhibited increased DNA damage and cancer cell inhibition compared to the individual treatments. Moreover, the nanomedicine has great potential to suppress the metabolism of cancer cells including both mitochondrial respiration and glycolytic activity, with enhanced efficacy observed when targeted to the cell surface protein EGFR. Our findings indicated that co-delivery of ATM siRNA and DOX serves as a more efficient therapeutic avenue in cancer treatment than delivery of the single species and offers a potential route for synergistically enhanced gene therapy.

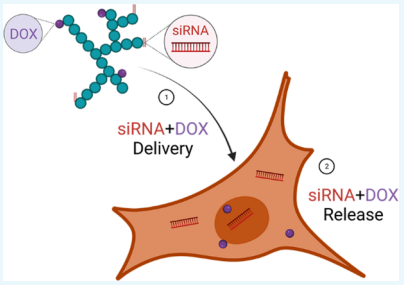

INTRODUCTION

siRNA is a powerful gene therapeutic that can knock down specific genes, disrupting cellular pathways that contribute to proliferation, drug resistance, and sensitivity and thereby cancer-related morbidity.[1,2] In many cases, using siRNA or the clinical standard chemotherapy as monotherapies may be insufficient to stop cancer progression due to resistance or insufficient delivery. However, combination therapies that involve co-delivery of siRNA together with anticancer drugs provide a promising approach to overcome chemoresistance.[3,4] Advantages of combining siRNA and chemotherapy include overcoming multidrug resistance (MDR), reducing off-target toxicity, and achieving potential synergistic apoptotic effects in tumorous cells.[5] Many studies have demonstrated that co-delivery of siRNA/miRNA and anticancer drugs via nanoparticle-based delivery systems can greatly enhance the inhibitory effect on tumor growth compared to siRNA or drug monotherapies.[6,7] Despite these initial advances in dual therapies using gene/chemotherapy, there obviously still exists a significant way to go before these systems are considered clinically viable and more work is required to better understand how the dual mechanisms of action provide enhanced therapeutic outcomes.

Ataxia-telangiectasia mutated (ATM) is a protein kinase that plays an important role in DNA response and cell cycle checkpoints.[8] With inactivated ATM gene and lack of the resulting kinase, cells are very sensitive to DNA-damaging agents.[9] Many studies have shown inhibition of breast cancer growth both *in vivo* and *in vitro* when the ATM gene has been targeted and silenced via treatment with an appropriate siRNA.[10,11] Doxorubicin (DOX) is one of the most effective chemotherapeutic drugs that is widely used in cancer treatment and functions by damaging DNA through preventing activity of topisomerase II.[12−15] In this study, a combination of ATM silencing siRNA and doxorubicin loaded into a hyperbranched polymer as a nanocarrier was investigated as a therapeutic strategy to treat breast cancer (Figure 1).

As shown in synthetic Scheme 1, a hyperbranched polymer (HBP) based on methacrylic monomers that contain primarily methoxy PEG pendant groups and small fractions of hydrazide,

Received: January 30, 2022
Accepted: April 26, 2022
Published: May 10, 2022

https://doi.org/10.1021/acsomega.2c00620
ACS Omega 2022, 7, 17119−17127

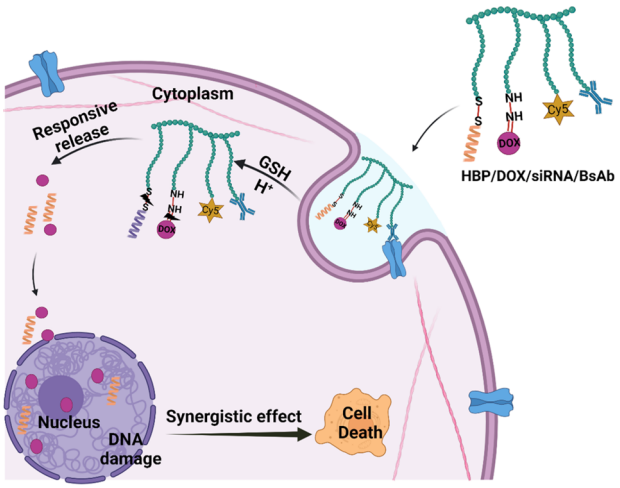

Figure 1. Schematic illustration of the proposed **HBP/DOX/siRNA/BsAb** behavior *in vitro*.

pyridine disulfide, and Cyanine 5 (Cy5) pendant groups forms the scaffold of the nanomedicine. The HBP was designed to include dual-responsive drug release mechanisms. DOX was attached via formation of a hydrazone bond between the ketone in DOX and the pendant hydrazides in the hyperbranched polymer, enabling pH-controlled release under mildly acidic conditions that mimic the pH of endosomal/lysosomal compartments of tumor cells (pH 4.0 to 6.5).[16−18] siRNA was attached to the hyperbranched polymer via a disulfide exchange reaction, which yielded a redox-sensitive disulfide linking group that could be cleaved under the highly reducing conditions encountered in the cytosol where glutathione (GSH) concentrations have been reported to range from 2−10 mM.[19−21] Moreover, the GSH concentration in the tumor microenvironment is up to 4 times higher than in normal tissues, providing a cell-specific release mechanism for the siRNA.[22,23] In order to track the polymer nanoparticles, cyanine 5 (Cy5) was also incorporated into the polymer as a fluorescent imaging tracer. In this study, a bispecific antibody (BsAb) with dual specificity for both methoxy PEG (mPEG) chains and epidermal growth factor receptor (EGFR) was bound to the mPEG containing the hyperbranched polymer as a targeting moiety.[24] This strategy takes advantage of the high expression of EGFR in many solid tumors and offers a simple and rapid route for customizing the cell target of the nanomedicine.[25,26] Therefore, as a potential route to overcome some of the issues associated with MDR, we report here a preliminary study investigating a theranostic nanoparticle that includes the combination of DOX and siRNA as a synergistic therapeutic against breast cancer.

EXPERIMENTAL SECTION

Materials. Human ATM gene-specific siRNA (ataxia-telangiectasia mutated sequence: sense: 5′-GGCCCUUAA-GUUAUUUGAAGAUA and anti-sense: 5′-UAUCUU-CAAAUAACUUA AGGGCC) were purchased from Bioneer Pacific. Doxorubicin hydrochloride, trifluoroacetic acid (TFA), triethylsilane, methacryloyl chloride, 2-mercaptoethanol, 2,2′-dithiodipyridine, *tert*-butyl carbazate, 4-dimethylaminopyridine (DMAP), 1-ethyl-3-(3-dimethylaminopropyl) carbodiimide hydrochloride (EDC·HCl), and 4,4′-azobis(4-cyanopentanoic acid) were bought from Sigma Aldrich and used directly without purification. Cyanine-5 amine was purchased from Lumiprobe. Azobis(isobutyronitrile) (AIBN, Sigma Aldrich) was recrystallized twice from methanol before use. Solvents including *n*-hexane, ethyl acetate, dichloromethane (DCM), dimethylformamide (DMF), diethyl ether, tetrahydrofuran, acetonitrile, and methanol were used dry where applicable and were of reagent grade quality. Poly((ethylene glycol)methyl ether methacrylate) (PEGMA, MW = 475 g·mol^{-1}) and ethylene glycol dimethacrylate (EGDMA) were purified to remove radical inhibitors before use by passing through a basic alumina column. Ultrapure water (18.2 MΩ cm) was obtained from an Elga ultrapure water system.

All products that are related to cell biology including cell culture media Dulbecco's modified Eagle's medium (DMEM), fetal bovine serum, (FBS), penicillin−streptomycin antibiotic solution, trypsin, trypan blue solution, phosphate saline buffer (PBS), sodium pyruvate, and glucose were purchased from Sigma, USA. MDA-MB-468 was incubated at 37 °C in a humidified atmosphere of 5% CO_2 in air.

Characterization. ^{1}H NMR spectra were acquired on a Bruker Avance 400 MHz spectrometer. A gel permeation chromatography−multiangle laser light scattering (GPC-MALLS) system consisting of a 1515 isocratic pump (Waters), Styragel HT 6E and Styragel HT 3 columns (Waters), a 2414 differential refractive index detector (Waters), and a Dawn Heleos multi angle laser light scattering detector (Wyatt) with THF as an eluent at a flow rate of 1 mL/min was used to measure the molecular weight and dispersity of the polymers. Dynamic light scattering (DLS) was used to measure the hydrodynamic diameter using a Malvern Zetasizer. Polyacrylamide gel electrophoresis (PAGE) was performed on a mini-Protean Tetra Cell equipped with a PowerPac Basic power supply at 100 V for 40 min in TBE buffer. 8% acrylamide and 8 M urea were used to make hand-cast gels. SYBR gold-stained gels were used for visualization and were carried out on a Gel Doc EZ System.

Synthesis of the Hyperbranched Polymer Carriers. The synthesis of poly(PEGMA-*co*-TBMC-*co*-pyridindisulfide-*co*-EDGMA-*co*-Cy5 MA) (**HBP-1**), deprotection of the *tert*-butyloxycarbonyl groups (**HBP-2**), and attachment of doxorubicin (**HBP/DOX**) follow the strategies reported in our previous study and are outlined schematically in Scheme 1.[27] The detailed synthetic procedure and all the characterization of the polymeric carrier including ^{1}H NMR, UV/Vis, and TEM are also listed in our published work.[27,28]

Conjugation of siRNA to the Hyperbranched Polymer, HBP/DOX/siRNA. Deprotection of siRNA was achieved by adding an appropriate volume of TCEP in TEAM buffer (5 mg/mL) to 10 μL of stock RNA solution (mole ratio TCEP:RNA = 20:1) in a 600 μL Eppendorf tube. Then, the mixture was vortexed for 30−60 s and incubated for 1 h at RT. After, the deprotected 5′-thiol-modified sense strand RNA was conjugated to either **HBP-2** or **HBP/DOX** via a disulfide exchange reaction using a thiol to pyridyl disulfide (PDS) ratio of 1:100. **HBP/DOX** or **HBP-2** (116 nmol, 4PDS group per **HBP-2**) was mixed with 5′-thiol-modified sense strand RNA (7 nmol) using siRNA-free water as a solvent at pH 8.0, by addition of an appropriate amount of 1.0 M triethylammonium bicarbonate (TEAB) buffer and incubating for 3 h at 25 °C. Then, **HBP/siRNA** and **HBP/DOX/siRNA** were purified by a G25 SEC column using PBS as an eluent buffer. The conjugation efficiency was determined using denaturing RNA urea-PAGE (4.8 g of urea, 3.75 mL of 20% acrylamide, 33 μL of 30% APS, 4 μL of TEMED, 1 mL 10× TBE). Successful

https://doi.org/10.1021/acsomega.2c00620
ACS Omega 2022, 7, 17119−17127

Scheme 1. Synthetic Scheme Showing the Development of a Dual Responsive Therapeutic for Delivery of Both Gene- and Chemotherapeutics

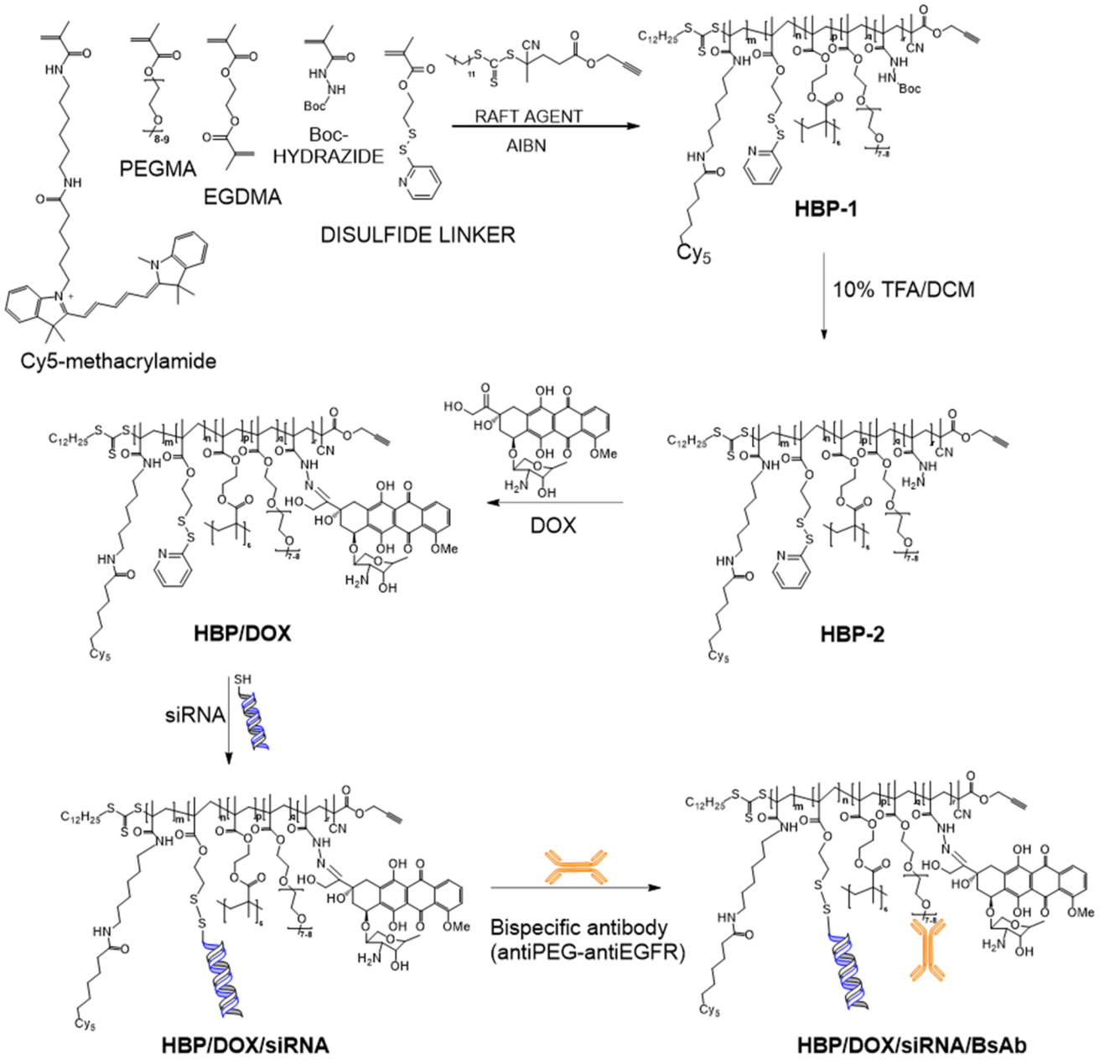

conjugation (80% coupling efficiency) was also confirmed by the appearance of multiple peaks of conjugated ssRNA in the HPLC chromatogram shown in Supporting Information, Figure S1, which was obtained using a Gemini reversed phase C18 column running an acetonitrile gradient 1−15% in a pH 9 $KHCO_3$ buffer. In order to form the targeted formulation, HBP/DOX/siRNA was mixed with BsAb at a molar ratio of 3:1 at room temperature for 30 min in PBS buffer to form HBP/DOX/siRNA/BsAb using strategies employed previously.[24,27]

Release Study. The release studies of both **HBP/siRNA** and **HBP/DOX/siRNA** were undertaken for 20 min at 37 °C in PBS buffer (pH = 7.4) in the presence of tris(2-carboxyethyl)phosphine (TCEP) at a concentration of 5 mg/mL as the reducing agent, and release was confirmed by PAGE analysis. Polyacrylamide gel electrophoresis of **HBP/siRNA** and **HBP/DOX/siRNA** conjugates was conducted on samples with or without TCEP treatment, with free siRNA as the control. The lanes were loaded with sample amounts that corresponded to 150 ng of siRNA. The gels were imaged after staining with SYBR gold nucleic acid gel stain (Gel Doc EZ System).

Real-Time Cell Proliferation Analysis. MDA-MB-468 breast cancer cells were pre-seeded into 96-well plates (5×10^3 cells/well). After incubation for 24 h at 37 °C, the DMEM culture medium was removed, and fresh medium was added. To investigate the dose response, the cells were then separately treated with **HBP/DOX/siRNA/BsAb**, **HBP/DOX/siRNA**, **HBP/DOX**, **HBP/siRNA**, free RNA, and free DOX. Cells were then monitored using the Incucyte Zoom Live Cell Analysis system (Essen, MI, USA), and images were taken at regular intervals during 144 h incubation at 37 °C with 5%

https://doi.org/10.1021/acsomega.2c00620
ACS Omega 2022, 7, 17119−17127

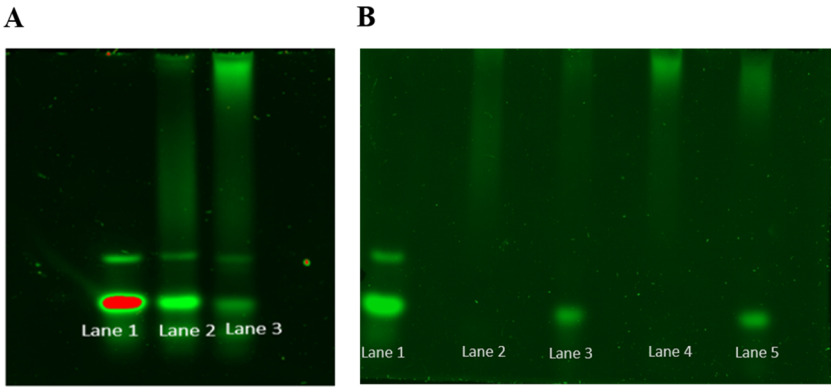

Figure 2. (A) Agarose gel electrophoresis of conjugates. Lane 1, 300 ng of free siRNA, lane 2, crude HBP/siRNA containing 300 ng siRNA directly after conjugating reaction, lane 3, crude HBP/DOX/siRNA containing 300 ng siRNA after conjugating reaction. Note that no purification reaction was performed on these products. Gels were made using 8% polyacrylamide, and electrophoresis was run at 100 V for 40 min and stained with SYBR gold. The red line in the first lane on the gel is due to oversaturation. (B) Agarose gel electrophoresis of HBP/siRNA and HBP/DOX/siRNA conjugates with or without TCEP treatment. The conjugate was preincubated for 20 min at 37 °C with TCEP at a concentration of 5 mg/mL. Lane 1, 150 ng of siRNA, lane 2, corresponding of 150 ng of siRNA of pure HBP/siRNA, lane 3, HBP/siRNA conjugate after treatment with TCEP, lane 4, corresponding 150 ng of siRNA of pure HBP/DOX/siRNA, lane 5, HBP/DOX/siRNA conjugate after treatment with TCEP. Visualization of gold SYBR-stained 8% acrylamide-urea gel.

CO_2. Cell proliferation curves were then plotted with the Incucyte Zoom software.

Study of the Effect of the Treatments on Cell Metabolism. After incubation of MDA-MB-468 cells in a 96-well plate at 5×10^4 cells/well in 200 μL of cell culture medium for 12 h, each formulation of nanoparticles was added to individual wells to give the same concentration of siRNA (150 ng/well) and/or DOX (2 μg mL^{-1}) and incubated for a further 24 h. Then, each of the wells was washed with Seahorse assay medium, which consisted of 1 mM sodium pyruvate and 25 mM glucose based on the manufacturer's assay instructions and 200 μL of fresh assay medium was added followed by CO_2-free incubation for another 1 h. The oxygen consumption rate (OCR) and extracellular acidification rate (ECAR) were measured using a Seahorse XF96 extracellular flux analyzer (Seahorse Bioscience) before and after the injection of oligomycin (1 μM) and carbonyl cyanide 4-(trifluoromethoxy) phenyl hydrazone (FCCP) (1 μM) into each well. All experiments were performed in at least triplicate.

siRNA Knock Down Study by Western Blot. Expression of ATM protein kinase was assessed by western blot analysis. MDA-MB-468 cells were seeded in 6-well plates (1×10^5 cells/well) and incubated in DMEM culture medium at 37 °C for 24 h. Then, each formulation of nanoparticles was added to give the same amount of siRNA (100 ng per 20 μL) for 24 h, washed with PBS, and harvested with versine after washing with warm PBS and incubation for 72 h. Protein samples were prepared from cell lysate for SDS-PAGE. Protein samples were diluted using Milli-Q water, and 50 μg of protein per 20 μL was loaded to each lane of an SDS-polyacrylamide gel, separated by electrophoresis, and then transferred to polyvinylidene fluoride (PVDF) membranes. The PVDF membranes were blocked with a blocking buffer, 5% bovine serum albumin (BSA), at 4 °C and then incubated with primary antibodies (anti-ATM, 1:1000), while a rabbit anti-β-actin antibody (1:1000) was used as a loading control. After sufficient washing, the membranes were incubated with goat anti-mouse polyclonal secondary antibodies (1:5000) in the dark for 1 h (Odyssey). After washing and drying, the membranes were scanned with the Odyssey CLx (LI-COR, NE, USE) imaging system, and Image J was used to analyze the protein band.

DNA Damage γ-H2AX Foci Measurement. Cells were cultured in 96-well plates with Lumox bases (Sarstedt). After drug treatment, the cells were fixed with 4% paraformaldehyde and permeabilized with Triton X-100. The cells were then incubated with γ-H2AX primary antibodies at 37 °C with 5% CO_2 followed by Alexa488-labeled secondary antibodies and DAPI to stain for DNA damage and nuclei. The stained cells were imaged using the INCell analyzer 2000 from GE Healthcare.

Statistical Analysis. All experimental data were obtained in triplicate unless otherwise mentioned and are presented as the mean ± standard deviation. Statistical comparison by analysis of variance was performed using Student's t test, and significance levels are reported in the text for each analysis. *P values < 0.05, **P values < 0.01, *** P values < 0.001, and **** P values < 0.0001 were considered statistically significant.

RESULTS AND DISCUSSION

The development of nanomedicines that can selectively release different therapeutics imparts stringent requirements in the design protocols. This is even more important when biomolecules are to be released because often they are incompatible with many of the chemistries required to undertake the different coupling approaches to assemble the nanomedicines. This can be complicated further when a molecular drug is combined with a biological drug (e.g., siRNA) and a biological targeting ligand (e.g., BsAb) as well as imaging agents for tracking the therapeutic under biological conditions. In this study, we have utilized orthogonal chemistries to formulate the multicomponent nanomedicine scaffold and then utilized antigenic interactions to establish a strong link between the targeting moiety (anti-EGFR) and the polymer using bispecific antibodies.

Synthesis and Release Study. The synthesis and release study of **HBP/DOX** nanomedicine has previously been well established and validated within our group.[27] These materials can be produced through facile synthetic approaches and have demonstrated release of DOX over 24 h in the acidic

https://doi.org/10.1021/acsomega.2c00620
ACS Omega 2022, 7, 17119−17127

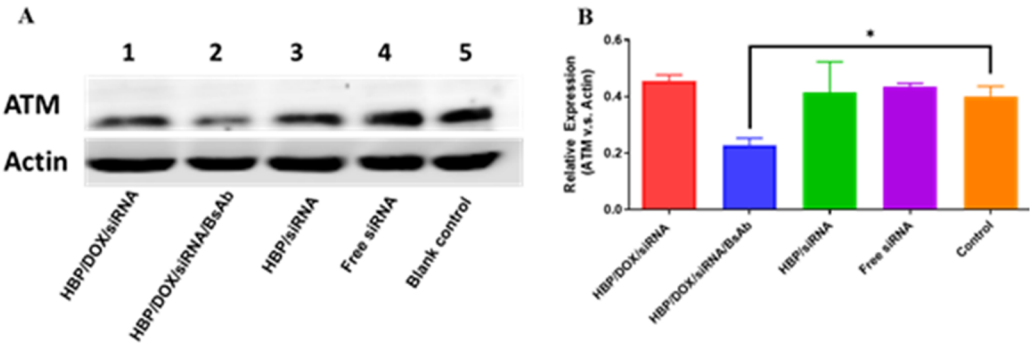

Figure 3. (A) Western blot of ATM expression in MDA-468 cells at 72 h post-transfection for **HBP/DOX/siRNA/BsAb**, **HBP/DOX/siRNA**, **HBP/siRNA**, free siRNA, and blank control. β-Actin was used as the internal control. (B) Relative expression levels of ATM compared to the β-actin internal control for cells treated with **HBP/DOX/siRNA/ BsAb**, **HBP/DOX/siRNA**, **HBP/siRNA** free siRNA, and the blank control ($n = 3$) ($^*p < 0.05$).

environment encountered during endosomal/lysosomal trafficking to effectively deliver the chemotherapeutic payload.

Building on this strategy, here we have sought to conjugate both the DOX chemotherapeutic with a gene-modifying component, siRNA. Hence, siRNA against ATM was conjugated to **HBP/DOX** or **HBP-2** for the single therapeutic species via the thiol-disulfide exchange reaction. As shown in Scheme 1, siRNA was successfully conjugated onto **HBP/DOX** where pyridyl disulfide groups of **HBP/DOX** were replaced by thiolated siRNA and formulated as **HBP/DOX/siRNA**. This approach has been demonstrated in the literature to be an effective means of attaching biomolecules to synthetic materials.[29,30]

Covalent conjugation of siRNA to the polymer systems (**HBP/DOX/siRNA** and **HBP/siRNA**) was confirmed by agarose gel electrophoresis of the crude product (Figure 2A). In the PAGE analyses, the increase in molecular weight due to formation of hyperbranched polymer-siRNA conjugates (lanes 2 and 3 in Figure 2A) prevented migration of the conjugate through the gel. Conversely, the lower-molecular-weight free siRNA (Lane 1, Figure 2A) migrated to the base of the gel (intense band), where the less intense band higher in the gel is likely due to a small amount of siRNA dimer. It is important to note that rather than observing discrete migration bands, which is generally the case for biomolecules, the smeared bands in lanes 2 and 3 were attributed to the hyperbranched polymer component of the conjugates, where streaking results from migration of the overall negatively charged conjugate through the gel. In this case, the HBP/DOX/siRNA showed a higher coupling efficiency than the HBP/siRNA, potentially due to the changed physicochemical properties of the HBP carrier when DOX was pre-attached. Quantitative fluorescence measurements from the gel indicated that the conjugation efficiency was approximately 80%, suggesting efficient coupling of the siRNA to **HBP/DOX** to form **HBP/DOX/siRNA**. The crude **HBP/siRNA** and **HBP/DOX/siRNA** were then purified using a G25 SEC column using PBS buffer as an eluent, and the resulting PAGE analysis showed an intense streaked band at the top of the gel for **HBP/siRNA** and **HBP/DOX/siRNA** (Figure 2B, lanes 2 and 4, respectively), with no band observed for free siRNA compared to lane 1 for the free siRNA. Following purification, the final polymer had approximately 0.8 siRNA molecules per HBP, slightly below the target 1 per HBP.

In order to validate whether the siRNA could be effectively released from the conjugate under reducing conditions, the samples were incubated with TCEP as the reducing agent to mimic the physiologically relevant conditions of high glutathione concentration in tumor cells.[29,31] After incubation with TCEP for 20 min, the siRNA was released from both the **HBP/siRNA** and **HBP/DOX/siRNA**, as shown in Figure 2B (lanes 3 and 5). This confirmed that siRNA could be successfully cleaved from the polymer conjugates in a reducing environment but was stable under non-reducing conditions. To further validate successful conjugation, HPLC chromatography with UV detection at 260 nm was used to confirm that free siRNA was not present in the conjugate. Supporting Information, Figure S1 shows the resulting HPLC trace of the free siRNA where an intense narrow peak was observed (green trace) at approximately 20 min retention time. This peak was not present in the spectrum for the conjugate and there was a shift of the peak to 27 min due to the formation of the higher-molecular-weight conjugate (purple trace). The strong baseline signals present in the HPLC traces were due to high absorbance of the buffer, and broadening of the peaks could be associated with the molecular dispersity of the hyperbranched polymer.

siRNA Knock Down Western Blot Study. The BsAb functionalization of HBP nanomedicines has been well studied and reported by our group. In short, tandem ScFv bispecific constructs are produced, whereby one binding site recognizes the disease epitope of interest, while the other binds to PEG. These BsAbs then decorate the surface of PEGylated nanomaterials through a simple mixing reaction under physiological conditions to produce a non-covalent targeted construct. This approach was used in the present study to produce targeted constructs of each DOX/siRNA-loaded HBP nanomaterial to assess the influence of targeting on subsequent efficacy.

The *in vitro* transfection efficiency of **HBP/DOX/siRNA/BsAb**, **HBP/DOX/siRNA**, **HBP/siRNA**, and free siRNA toward MDA-MB-468 cells was evaluated via western blot analysis. The proteins were transferred from the SDS PAGE gel to a PVDF gel, incubated with a primary antibody for ATM, and then stained. Actin was used as a control. As shown in Figure 3, only **HBP/DOX/siRNA/BsAb** showed a statistically significant reduction in ATM/actin in the cells, compared to either **HBP/DOX/siRNA** or **HBP/siRNA**. This suggests that BsAb is facilitating transport of the nanoparticles into the cells with the requisite endosomal escape of the siRNA to allow it to enact gene knockdown. This data indicated that

https://doi.org/10.1021/acsomega.2c00620
ACS Omega 2022, 7, 17119−17127

HBP/DOX/siRNA/BsAb could successfully be used as an siRNA delivery system, which can reduce expression of ATM.

***In Vitro* Cell Viability.** Next, we investigated whether the conjugates and scaffold controls could influence cell proliferation in MDA-MB-468 breast cancer cells and the real-time percent confluence versus proliferation time plots are shown in Figure 4. Dual and single therapy controls were assessed at

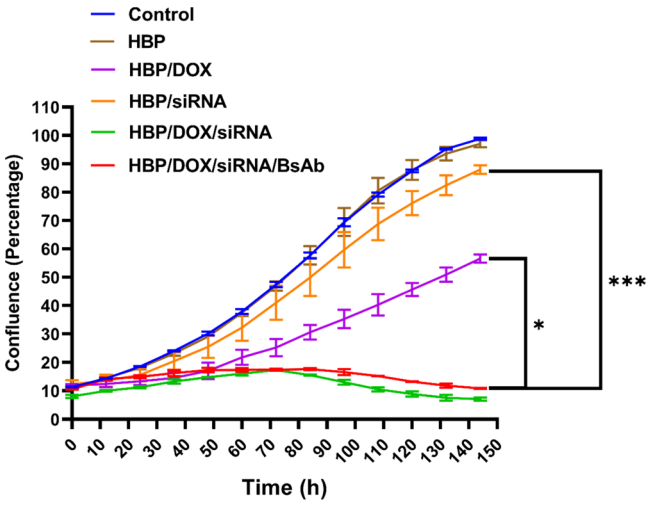

Figure 4. Cell proliferation studies for treatment of MDA-MB-468 cells with **HBP**, **HBP/DOX**, **HBP/siRNA**, **HBP/DOX/siRNA**, **HBP/DOX/siRNA/BsAb**, and **HBP/BsAb**. Values are the means ± the standard deviations (n = 5, S.D.) (*p < 0.05, ***p < 0.001).

siRNA doses of 150 ng/mL and DOX at 2 μg mL^{-1}. Both **HBP/DOX/siRNA** and **HBP/DOX/siRNA/BsAb** showed the greatest inhibition of proliferation, where the percentage confluence did not exceed 18% and had confluences of less than 10% at 145 h. This was significantly lower when compared to **HBP/DOX** without siRNA, which reached 40% confluence at 145 h for an equivalent concentration of DOX in the sample. These results indicated that a combination of siRNA and DOX improved therapeutic efficacy compared to single-therapeutic variants. Importantly, the therapeutic-free HBP scaffold did not show any significant toxicity toward the cells compared to the saline control, where both reached 100% confluence at 145 h of proliferation. In addition, only a minimal decrease in proliferation (85% confluence at 145 h) was observed for **HBP/siRNA** at siRNA doses of 150 ng. The data suggest that the siRNA and DOX combined act in concert to improve the therapeutic response of the nanomedicine formulations.

DNA Damage γ-H2AX Foci. γ-H2AX is a phosphorylated version of H2AX (a histone H2A variant) that forms after double-strand breaks (DSBs) of DNA.[32] The γ-H2AX and other proteins then aggregate into foci as part of the cellular response to DNA damage. Visualizing and quantifying the number of γ-H2AX foci using fluorescence microscopy has become a recognized method for assessing the extent of DNA damage in cells.[33]

Figure 5A shows representative fluorescence microscopy images of MDA-MB-468 cells treated with a series of hyperbranched polymers conjugated with different combinations of siRNA, DOX, and BsAb as well as numerous controls. Figure 5B compares the images by plotting the percentages of cell populations that have more than 5 γ-H2AX foci in the

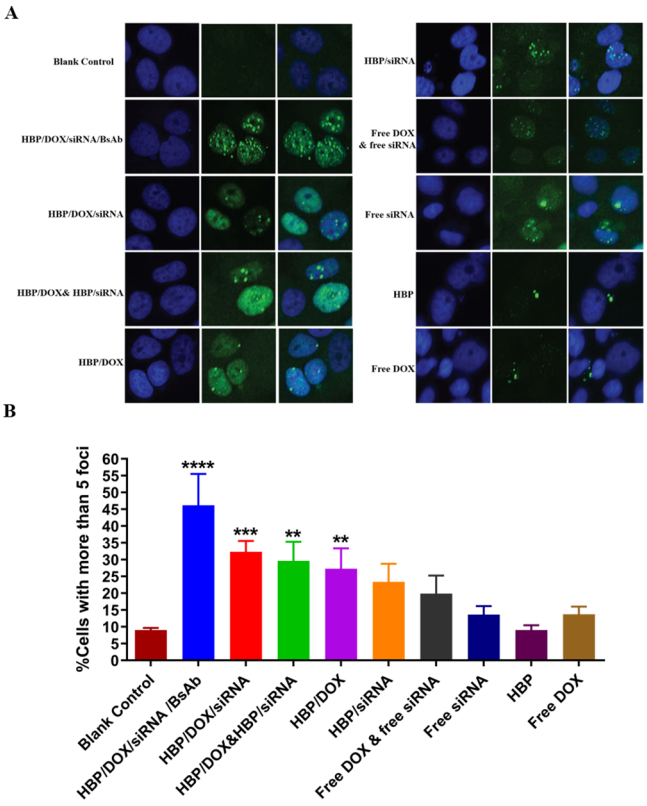

Figure 5. (A) Cell DNA damage γ-H2AX foci study detected by immunocytochemical staining for γ-H2AX (green) and DNA counterstaining with DAPI (blue) in MDA-MB-486 cells. (B) Percentage of cell foci determined by image analysis. Values are the means ± the standard deviations (n = 5, S.D.) and compared with blank control (**p < 0.01, ***p < 0.001, ****p < 0.0001).

nucleus. The cells treated with the fully formulated nanomedicine, **HBP/DOX/siRNA/BsAb**, had the highest yields of the γ-H2AX foci with 45 ± 9% of the cells having more than 5 foci in the nucleus compared to the control, which only had 8 ± 1% of the cells with more than 5 foci (****p < 0.0001, n = 5). Treatment with **HBP/DOX/siRNA/BsAb** was also significantly higher than **HBP/siRNA** and the free drugs, which had 12−22%.

To compare whether the dual-therapy approach was influenced by being contained within a single scaffold or simply simultaneously delivered in nanomaterials applied at the same time, the DNA damage of **HBP/DOX/siRNA** and combinations of individual therapy construct **HBP/DOX** & **HBP/siRNA** was compared. **HBP/DOX/siRNA** and **HBP/DOX** & **HBP/siRNA** showed high yields of γ-H2AX foci, with 32 ± 3% and 29 ± 5% of the cells exhibiting greater than 5 foci. This may be due to siRNA blocking the ATM gene and resulting kinase, thus leading to the great sensitivity of cells to DNA-damaging agent DOX, although this was lower than the fully formulated nanomedicine showing the importance of targeting BsAb.

Influence of the Nanomedicines on Cell Metabolism. Cell metabolism including mitochondrial oxidative phosphorylation and glycolysis plays essential roles in tumorigenesis. In our study, the focus has been to treat MDA-MB-468 breast cancer cells with different formulations of HBP nanomedicines and then assess the effect on mitochondrial respiration and glycolytic activity via measuring the oxygen consumption rate

https://doi.org/10.1021/acsomega.2c00620
ACS Omega 2022, 7, 17119−17127

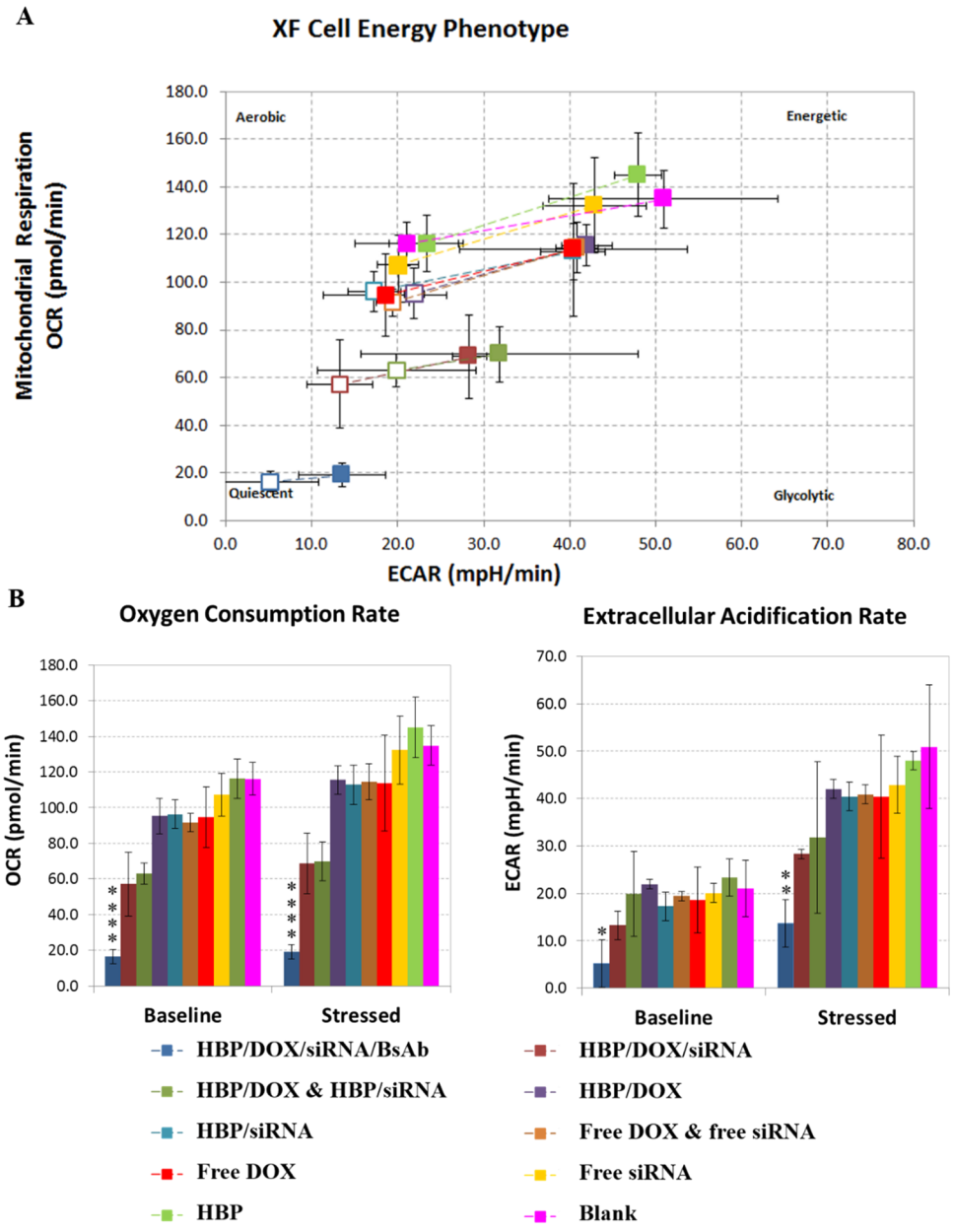

Figure 6. Analysis of mitochondrial bioenergetics of MDA-MB-468 cells that have been treated with the following formulations: **HBP**, **HBP/DOX**, **HBP/siRNA**, **HBP/DOX/siRNA**, **HBP/DOX/siRNA/BsAb**, and **HBP/BsAb** against MDA-MB-468 cells at concentrations corresponding to 2 μg mL^{-1} DOX and free siRNA at loading corresponding to 150 ng. (A) Mitochondrial respiration of cell energy phenotype. (B) Oxygen consumption rate and extracellular acidification rate. Values are the means ± standard deviations (n = 5, S.D.) and compared with blank control (*p < 0.05, **p < 0.01, ****p < 0.0001).

(OCR) and extracellular acidification rate (ECAR) before (baseline measurement) and after being stressed by addition of oligomycin and FCCP. The oligomycin inhibits mitochondrial production of ATP causing an increase in the rate of glycolysis, while FCCP functions by depolarizing the mitochondrial membrane, which increases the rate of oxygen consumption. Hence, the measurements provide information regarding the baseline energy requirements for the cells, the stressed phenotype under an induced energy demand, and the difference, which is the metabolic potential.[27]

MDA-MB-468 cells were treated with different formulations of nanoparticles for 24 h and the level of oxygen consumption was assessed using a Seahorse XF extracellular flux analyzer. **HBP/DOX/siRNA/BsAb** exhibited a significantly reduced oxygen consumption rate compared to the control for the baseline and stressed conditions and was the lowest OCR of the sample group. The extracellular acidification rate (ECAR) was also the lowest, indicating that the fully formulated nanomedicine had the highest potential for reducing glycolytic activity. The above results indicate that when treated with **HBP/DOX/siRNA/BsAb**, MDA-MB-468 cells are significantly less energetic compared to the control and also to the other treatment groups, where the treatment has effectively rendered the cells into a quiescent state. Stressing the cells by addition of oligomycin and FCCP showed no significant increase in OCR (20 pmol/min increase for control) and only a 10 mpH/min increase in the ECAR (30 mpH/min increase for control) and an overall metabolic potential that was

https://doi.org/10.1021/acsomega.2c00620
ACS Omega 2022, 7, 17119−17127

reduced compared to the control. This indicated that cancer cell deaths may be related to the ability of the targeted therapeutic **HBP/DOX/siRNA/BsAb** to inhibit the cellular energy status.

HBP/DOX/siRNA and **HBP/siRNA** & **HBP/DOX** reduced the metabolic activity compared to the control, but the metabolic activity was higher than that for **HBP/DOX/siRNA/BsAb** (Figure 6). Similar to the DNA damage results described above, having the combination of the targeting BsAb, DOX, and siRNA gives the highest therapeutic efficacy. It is expected that this is due to BsAb facilitating facile internalization of the siRNA and DOX into the cells and potentially leading to favorable intracellular trafficking of the therapeutic components.

CONCLUSIONS

In summary, we have successfully developed a theranostic system via attaching various functional molecules including a bispecific antibody as a targeting agent and Cy5 as an imaging tracer and then incorporation of doxorubicin and siRNA as therapeutics using stimulus-cleavable chemical linkages. Moreover, the siRNA attachment was very efficient, where more than 80% available sites were conjugated with siRNA. In addition, we have demonstrated that the majority of siRNA could be released *in vitro* under reducing conditions. We have further investigated cellular toxicity and shown that **HBP/DOX/siRNA/BsAb** could significantly inhibit cell growth compared to either **HBP/DOX** or **HBP/siRNA** control groups. Furthermore, **HBP/DOX/siRNA/BsAb** showed greatest inhibition of both mitochondrial respiration and glycolytic activity from metabolic studies. While the combination of chemo−gene therapies showed enhanced effect in cell studies, further optimization of the chemo:gene ratio would be required to fully exploit this effect. Overall, all these features indicate that this **HBP/DOX/siRNA/BsAb** system is a promising theranostic for understanding novel treatment mechanisms for breast cancer therapy.

ASSOCIATED CONTENT

Supporting Information

The Supporting Information is available free of charge at https://pubs.acs.org/doi/10.1021/acsomega.2c00620.

HPLC and NMR data for polymers at different stages of formulation; table of physicochemical properties; UV−Vis spectra of drug-loaded polymers (PDF)

AUTHOR INFORMATION

Corresponding Author

Kristofer J. Thurecht − *Centre for Advanced Imaging, Australian Institute for Bioengineering and Nanotechnology, ARC Centre of Excellence in Convergent Bio-Nano Science and Technology and ARC Training Centre in Biomedical Imaging Technology, The University of Queensland, Brisbane, QLD 4072, Australia;* orcid.org/0000-0002-4100-3131; Email: k.thurecht@uq.edu.au

Authors

Yongmei Zhao − *School of Pharmacy, Nantong University, Nantong 226019, China*

Tianqing Liu − *QIMR Berghofer Medical Research, Brisbane, QLD 4006, Australia;* orcid.org/0000-0002-9058-2643

Aditya Ardana − *Commonwealth Scientific and Industrial Research Organisation, Canberra 2601, Australia*

Nicholas L. Fletcher − *Centre for Advanced Imaging, Australian Institute for Bioengineering and Nanotechnology, ARC Centre of Excellence in Convergent Bio-Nano Science and Technology and ARC Training Centre in Biomedical Imaging Technology, The University of Queensland, Brisbane, QLD 4072, Australia;* orcid.org/0000-0002-2993-833X

Zachary H. Houston − *Centre for Advanced Imaging, Australian Institute for Bioengineering and Nanotechnology, ARC Centre of Excellence in Convergent Bio-Nano Science and Technology and ARC Training Centre in Biomedical Imaging Technology, The University of Queensland, Brisbane, QLD 4072, Australia;* orcid.org/0000-0001-9738-4917

Idriss Blakey − *Centre for Advanced Imaging, Australian Institute for Bioengineering and Nanotechnology, ARC Centre of Excellence in Convergent Bio-Nano Science and Technology and ARC Training Centre in Biomedical Imaging Technology, The University of Queensland, Brisbane, QLD 4072, Australia;* orcid.org/0000-0003-2389-6156

Complete contact information is available at: https://pubs.acs.org/10.1021/acsomega.2c00620

Author Contributions

#Y.Z. and T.L. contributed equally.

Notes

The authors declare no competing financial interest.

ACKNOWLEDGMENTS

Y.Z. is supported by the National Science Foundation of the Jiangsu Higher Education Institutions of China (Grant No. 19KJD350002) and Jiangsu's Mass Entrepreneurship and Innovation Program. We acknowledge the National Health and Medical Research Council for fellowship support (K.J.T.; APP1148582). This work was performed in part at the Queensland node of the Australian National Fabrication Facility (ANFF), a company established under the National Collaborative Research Infrastructure Strategy to provide nano- and microfabrication facilities for Australia's researchers. Research was funded through the ARC Centre of Excellence in Convergent BioNano Science and Technology (CE140100036) and in part by the ARC Training Centre for Innovation in Biomedical Imaging Technologies (IC170100035).

REFERENCES

(1) Hu, B.; Zhong, L.; Weng, Y.; Peng, L.; Huang, Y.; Zhao, Y.; Liang, X. J. Therapeutic siRNA: state of the art. *Signal Transduction Targeted Ther.* **2020**, *5*, 101.

(2) Bholakant, R.; Qian, H.; Zhang, J.; Huang, X.; Huang, D.; Feijen, J.; Zhong, Y.; Chen, W. Recent Advances of Polycationic siRNA Vectors for Cancer Therapy. *Biomacromolecules* **2020**, *21*, 2966−2982.

(3) Ashrafizadeh, M.; Zarrabi, A.; Hushmandi, K.; Hashemi, F.; Rahmani Moghadam, E.; Raei, M.; Kalantari, M.; Tavakol, S.; Mohammadinejad, R.; Najafi, M.; Tay, F. R.; Makvandi, P. Progress in Natural Compounds/siRNA Co-delivery Employing Nanovehicles for Cancer Therapy. *ACS Comb. Sci.* **2020**, *22*, 669−700.

(4) Xiong, X. B.; Lavasanifar, A. Traceable multifunctional micellar nanocarriers for cancer-targeted co-delivery of MDR-1 siRNA and doxorubicin. *ACS Nano* **2011**, *5*, 5202−5213.

(5) Zeinali, M.; Abbaspour-Ravasjani, S.; Ghorbani, M.; Babazadeh, A.; Soltanfam, T.; Santos, A. C.; Hamishehkar, H.; Hamblin, M. R. Nanovehicles for co-delivery of anticancer agents. *Drug Discovery Today* **2020**, *25*, 1416−1430.

(6) Khelghati, N.; Soleimanpour Mokhtarvand, J.; Mir, M.; Alemi, F.; Asemi, Z.; Sadeghpour, A.; Maleki, M.; Samadi Kafil, H.; Jadidi-Niaragh, F.; Majidinia, M.; Yousefi, B. The importance of co-delivery of nanoparticle-siRNA and anticancer agents in cancer therapy. *Chem. Biol. Drug Des.* **2021**, *97*, 997−1015.
(7) Yin, T.; Liu, Y.; Yang, M.; Wang, L.; Zhou, J.; Huo, M. Novel Chitosan Derivatives with Reversible Cationization and Hydrophobicization for Tumor Cytoplasm-Specific Burst Co-delivery of siRNA and Chemotherapeutics. *ACS Appl. Mater. Interfaces* **2020**, *12*, 14770−14783.
(8) Saraswathy, M.; Gong, S. Recent developments in the co-delivery of siRNA and small molecule anticancer drugs for cancer treatment. *Mater. Today* **2014**, *17*, 298−306.
(9) Shiloh, Y.; Ziv, Y. The ATM protein kinase: regulating the cellular response to genotoxic stress, and more. *Nat. Rev. Mol. Cell Biol.* **2013**, *14*, 197−210.
(10) Xu, R.; Huang, Y.; Mai, J.; Zhang, G.; Guo, X.; Xia, X.; Koay, E. J.; Qin, G.; Erm, D. R.; Li, Q.; Liu, X.; Ferrari, M.; Shen, H. Multistage vectored siRNA targeting ataxia-telangiectasia mutated for breast cancer therapy. *Small* **2013**, *9*, 1799−1808.
(11) Jerzak, K. J.; Mancuso, T.; Eisen, A. Ataxia-telangiectasia gene (ATM) mutation heterozygosity in breast cancer: a narrative review. *Curr. Oncol.* **2018**, *25*, e176−e180.
(12) Rafiei, S.; Fitzpatrick, K.; Liu, D.; Cai, M.-Y.; Elmarakeby, H. A.; Park, J.; Ricker, C.; Kochupurakkal, B. S.; Choudhury, A. D.; Hahn, W. C.; Balk, S. P.; Hwang, J. H.; Van Allen, E. M.; Mouw, K. W. ATM Loss Confers Greater Sensitivity to ATR Inhibition Than PARP Inhibition in Prostate Cancer. *Cancer Res.* **2020**, *80*, 2094−2100.
(13) Tacar, O.; Sriamornsak, P.; Dass, C. R. Doxorubicin: an update on anticancer molecular action, toxicity and novel drug delivery systems. *J Pharm. Pharmacol.* **2013**, *65*, 157−170.
(14) Fornari, F. A.; Randolph, J. K.; Yalowich, J. C.; Ritke, M. K.; Gewirtz, D. A. Interference by doxorubicin with DNA unwinding in MCF-7 breast tumor cells. *Mol. Pharmacol.* **1994**, *45*, 649−656.
(15) Momparler, R. L.; Karon, M.; Siegel, S. E.; Avila, F. Effect of adriamycin on DNA, RNA, and protein synthesis in cell-free systems and intact cells. *Cancer Res.* **1976**, *36*, 2891−2895.
(16) Hu, Y. B.; Dammer, E. B.; Ren, R. J.; Wang, G. The endosomal-lysosomal system: from acidification and cargo sorting to neurodegeneration. *Transl. Neurodegener.* **2015**, *4*, 18.
(17) Overly, C. C.; Lee, K. D.; Berthiaume, E.; Hollenbeck, P. J. Quantitative measurement of intraorganelle pH in the endosomal-lysosomal pathway in neurons by using ratiometric imaging with pyranine. *Proc. Natl. Acad. Sci. U. S. A.* **1995**, *92*, 3156−3160.
(18) Benjaminsen, R. V.; Sun, H.; Henriksen, J. R.; Christensen, N. M.; Almdal, K.; Andresen, T. L. Evaluating nanoparticle sensor design for intracellular pH measurements. *ACS Nano* **2011**, *5*, 5864−5873.
(19) Mura, S.; Nicolas, J.; Couvreur, P. Stimuli-responsive nanocarriers for drug delivery. *Nat. Mater.* **2013**, *12*, 991−1003.
(20) Cheng, R.; Meng, F.; Deng, C.; Klok, H. A.; Zhong, Z. Dual and multi-stimuli responsive polymeric nanoparticles for programmed site-specific drug delivery. *Biomaterials* **2013**, *34*, 3647−3657.
(21) Wu, G.; Fang, Y. Z.; Yang, S.; Lupton, J. R.; Turner, N. D. Glutathione metabolism and its implications for health. *J. Nutr.* **2004**, *134*, 489−492.
(22) Kuppusamy, P.; Li, H.; Ilangovan, G.; Cardounel, A. J.; Zweier, J. L.; Yamada, K.; Krishna, M. C.; Mitchell, J. B. Noninvasive imaging of tumor redox status and its modification by tissue glutathione levels. *Cancer Res.* **2002**, *62*, 307−312.
(23) Lin, W.; Guan, X.; Sun, T.; Huang, Y.; Jing, X.; Xie, Z. Reduction-sensitive amphiphilic copolymers made via multi-component Passerini reaction for drug delivery. *Colloids Surf., B* **2015**, *126*, 217−223.
(24) Howard, C. B.; Fletcher, N.; Houston, Z. H.; Fuchs, A. V.; Boase, N. R. B.; Simpson, J. D.; Raftery, L. J.; Ruder, T.; Jones, M. L.; de Bakker, C. J.; Mahler, S. M.; Thurecht, K. J. Overcoming Instability of Antibody-Nanomaterial Conjugates: Next Generation Targeted Nanomedicines Using Bispecific Antibodies. *Adv. Healthcare Mater.* **2016**, *5*, 2055−2068.
(25) Mendelsohn, J. Epidermal growth factor receptor inhibition by a monoclonal antibody as anticancer therapy. *Clin. Cancer Res.* **1997**, *3*, 2703−2707.
(26) Wee, P.; Wang, Z. Epidermal Growth Factor Receptor Cell Proliferation Signaling Pathways. *Cancers* **2017**, *9*, 52.
(27) Zhao, Y.; Fletcher, N. L.; Gemmell, A.; Houston, Z. H.; Howard, C. B.; Blakey, I.; Liu, T.; Thurecht, K. J. Investigation of the Therapeutic Potential of a Synergistic Delivery System through Dual Controlled Release of Camptothecin−Doxorubicin. *Adv. Ther.* **2020**, *3*, 1900202.
(28) Tan, J. H.; McMillan, N. A. J.; Payne, E.; Alexander, C.; Heath, F.; Whittaker, A. K.; Thurecht, K. J. Hyperbranched polymers as delivery vectors for oligonucleotides. *J. Polym. Sci., Part A: Polym. Chem.* **2012**, *50*, 2585−2595.
(29) Matsumoto, N. M.; González-Toro, D. C.; Chacko, R. T.; Maynard, H. D.; Thayumanavan, S. Synthesis of Nanogel-Protein Conjugates. *Polym. Chem.* **2013**, *4*, 2464−2469.
(30) Ardana, A.; Whittaker, A. K.; Thurecht, K. J. PEG-Based Hyperbranched Polymer Theranostics: Optimizing Chemistries for Improved Bioconjugation. *Macromolecules* **2014**, *47*, 5211−5219.
(31) Heredia, K. L.; Nguyen, T. H.; Chang, C. W.; Bulmus, V.; Davis, T. P.; Maynard, H. D. Reversible siRNA-polymer conjugates by RAFT polymerization. *Chem. Commun.* **2008**, 3245−3247.
(32) Collins, P. L.; Purman, C.; Porter, S. I.; Nganga, V.; Saini, A.; Hayer, K. E.; Gurewitz, G. L.; Sleckman, B. P.; Bednarski, J. J.; Bassing, C. H.; Oltz, E. M. DNA double-strand breaks induce H2Ax phosphorylation domains in a contact-dependent manner. *Nat. Commun.* **2020**, *11*, 3158.
(33) Lapytsko, A.; Kollarovic, G.; Ivanova, L.; Studencka, M.; Schaber, J. FoCo: a simple and robust quantification algorithm of nuclear foci. *BMC Bioinf.* **2015**, *16*, 392.

https://doi.org/10.1021/acsomega.2c00620
ACS Omega 2022, 7, 17119−17127